Engineering Geology 273 (2020) 105690

Contents lists available at ScienceDirect

Engineering Geology

journal homepage: www.elsevier.com/locate/enggeo

Surface traces and related deformation structures of the southern Sanyi Fault, Taiwan, as deduced from field mapping, electrical-resistivity tomography, and shallow drilling

Gong-Ruei Ho[a], Ping-Yu Chang[b,c], Jian-Cheng Lee[a,*], Jonathan C. Lewis[d], Po-Tsun Chen[e], Han-Lun Hsu[b]

[a] Institute of Earth Sciences, Academia Sinica, Taipei, Taiwan
[b] Department of Earth Sciences, National Central University, Zhongli, Taoyuan, Taiwan
[c] Earthquake-Disaster & Risk Evaluation and Management Center, E-DREaM, National Central University, Zhongli, Taoyuan, Taiwan
[d] Department of Geoscience, Indiana University of Pennsylvania, Indiana, PA, USA
[e] Central Geological Survey, MOEA, New Taipei, Taiwan

ARTICLE INFO

Keywords:
Sanyi Fault
Active fault
Electric resistivity
Multiple fault branch
Seismic hazards
City planning

ABSTRACT

The southern Sanyi Fault extends across a highly urbanized area in central-west Taiwan. It is within 1–2 km from and generally parallels the northern Chelungpu Fault, which last ruptured in 1999 (Mw = 7.6 Chi-Chi Earthquake) and caused about 2400 fatalities. Several questions thus arise: is the Sanyi Fault likewise active? what is its geometry and extent? and should it be zoned or otherwise designated to mitigate risk through restrictions on development or engineering design? We address these questions by mapping river-exposed outcrops, by interpreting nine, near-surface geophysical surveys (electrical resistivity tomography [ERT]), and by compiling and assessing existing shallow borehole data. Outcrops in the Dajia River show that the Sanyi Fault is mainly a low-angle thrust that juxtaposes poorly lithified sandstone over alluvial gravels. Fault branches are common both in the hanging wall and footwall. To the south, the fault is not marked by a break in topography and its trace has not been clearly mapped within the alluvial plain, in part motivating the current effort. Here the ERT surveys identify the hanging-wall sandstone by a relatively low resistivity of < 100 Ωm, whereas the footwall conglomerates and alluvial gravels generally exceed ~300 Ωm and ~ 100 Ωm, respectively. Borehole data likewise constrain the extent and character of the Sanyi Fault, which we identify as extending across the eastern part of Fengyuan, a city with a population now exceeding 160,000. The fault system is clearly imaged in two of five surveyed sites, and we integrate these data with drilling data to map the Sanyi fault surface trace as a ~ 400 m wide zone in the city of Fengyuan. Compiling previously documented paleoseismic data at one site, the Sanyi Fault system likely slipped in the thousand-year range throughout the Holocene. The Sanyi Fault is therefore 'active' and warrants zoning or other forms of mitigation to minimize potential, seismically induced loss of life and property.

1. Introduction

The 1999 Mw 7.6 Chi-Chi Earthquake resulted from the reactivation of the Chelungpu Fault in central western Taiwan and caused a huge loss of property and life (Kao and Chen, 2000; Lee et al., 2002). West central Taiwan is located in the active fold-and-thrust belt, which is characterized by 3 subparallel thrust systems, from west to east, the Changhua, Sanyi-Chelungpu, and Tamaopu-Shuangtung Faults (Fig. 1) (Ho, 1976; Suppe, 1981; Angelier et al., 1986; Hung and Wiltschko, 1993; Lee, 1994; Chen et al., 2000a, 2000b; Hung and Suppe, 2000; Y.G. Chen et al., 2001a; W.S. Chen et al., 2001b, 2003; Lin et al., 2002; Lai et al., 2006; Hung et al., 2009; Yue et al., 2005). As a consequence, better understanding of these three active thrusts is crucial for seismic hazards mitigation and city planning in this populated part of Taiwan. Fault studies aimed at hazard mitigation (e.g., Kim et al., 2011; Lee et al., 2014; Guerrieri et al., 2015; Juang et al., 2016) commonly rely on surface geological investigations, including shallow drilling, integrated geophysical surveys (Duffy et al., 2014; Kim et al., 2008), and/or geochemical analyses (Niwa et al., 2016, 2019).

In this study, we focused on the southern Sanyi Fault, where it is

* Corresponding author.
E-mail address: jclee@earth.sinica.edu.tw (J.-C. Lee).

https://doi.org/10.1016/j.enggeo.2020.105690
Received 20 November 2019; Received in revised form 15 May 2020; Accepted 15 May 2020
Available online 19 May 2020

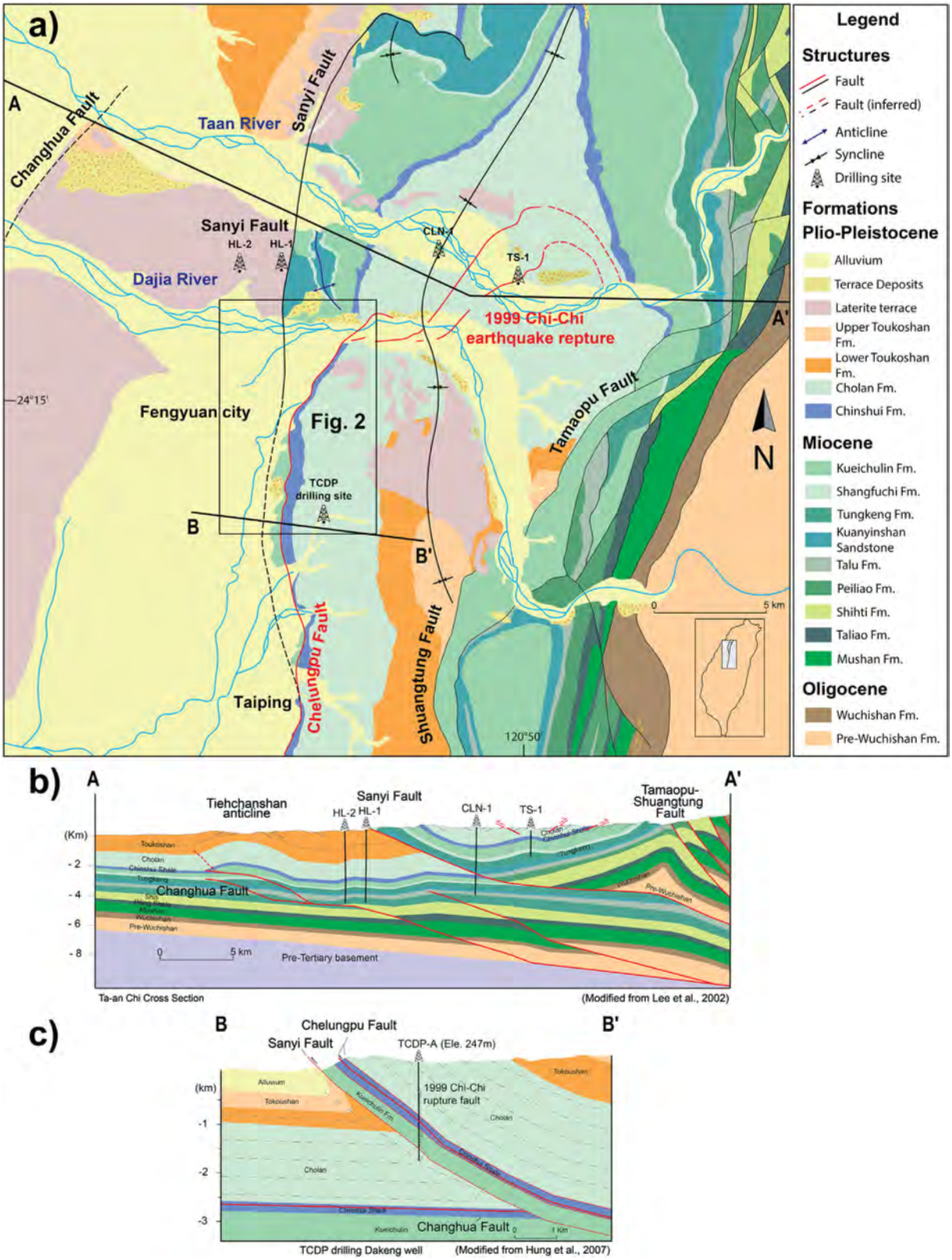

Fig. 1. (a) General geological map of the Sanyi-Chelungpu Fault system (after 1:100,000 map sheets, Chinese Petroleum Corporation (CPC), 1974; Miaoli sheet and, 1982 Taichung sheet). The Sanyi Fault is overlapping, in map view, and subparallel to the Chelungpu Fault for 10–12 km in the alluvial plain around the city of Fengyuan. (b) Interpreted geological cross section across the middle part of the Sanyi Fault (modified from Lee et al., 2002). In this area, the northernmost Chelungpu Fault gradually becomes shallower, following the trend of a regional south-plunging syncline, in the hanging wall of the Sanyi Fault. (c) Interpreted geological cross section across the southern Sanyi Fault at the site of the TCDP drilling Hole-A (modified from Hung et al., 2007). While the Chelungpu Fault ruptured as bedding-parallel slip within the Mio-Pliocene rock units, the southern Sanyi Fault shows a Miocene sandstone hanging wall flat on top of a footwall ramp in Quaternary conglomerate and alluvial deposits at the shallow level. The 1.7 km long TCDP drilling cores indicated that the Sanyi Fault and Chelungpu Fault are merely ~400 m away each other at the site area.

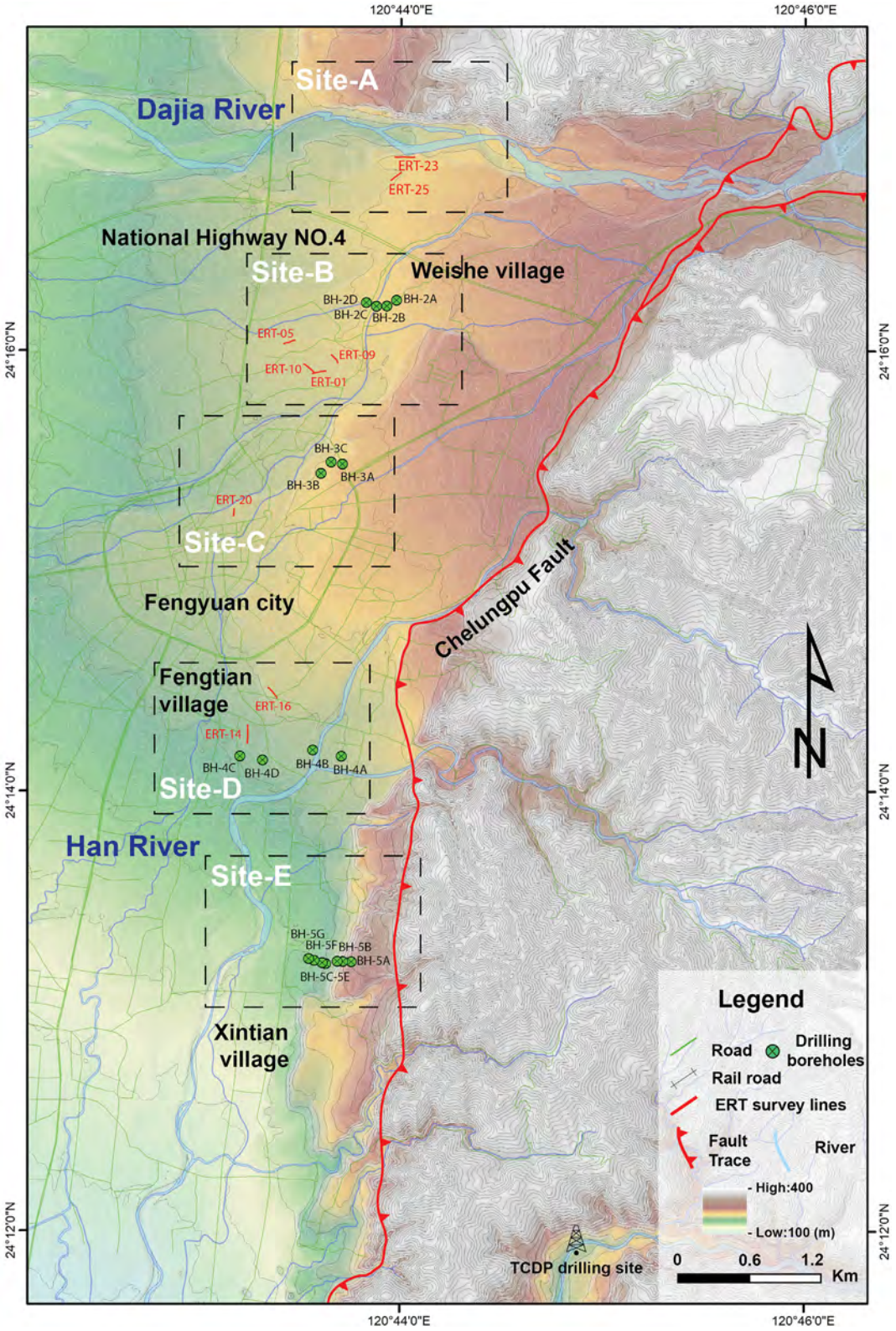

Fig. 2. Index map of study area on a 20-m DEM showing the topography. The five areas selected for detailed study by outcrop mapping, geophysical ERT imaging and synthesizing drilling and trenching data are outlined (Sites A, B, C, D and E). Green dots: shallow drilling boreholes. Red bars: ERT survey lines. (For interpretation of the references to colour in this figure legend, the reader is referred to the web version of this article.)

subparallel to the Chelungpu Fault for 10–12 km. The Taiwan Chelungpu fault Drilling Project (TCDP) Hole-A at the northern part of the Chelungpu Fault crossed the Sanyi Fault about 400 m below the Chelungpu thrust plane (Fig. 1c) (Hung et al., 2007). Drilling showed that the Sanyi and Chelungpu Faults are subparallel and occur within a few hundred meters of each other. From the regional geological point of view, the Sanyi Fault has accumulated significantly larger displacements than those on the Chelungpu Fault, therefore also has a high

potential earthquake risk. Our efforts also address the question of whether the Sanyi Fault could generate a disastrous earthquake like its neighbor the Chelungpu Fault next to it. To this end, it is important to locate the surface traces of the Sanyi Fault, particularly its southern end where it appears to transect the city of Fengyuan. However, the major limitation or challenge has been that the southern Sanyi Fault is exposed in only few outcrops and most of its surface trace is buried under alluvial deposits due to the high sedimentation rates (Dadson et al., 2003). Therefore, the detailed structural characteristics of the Sanyi Fault at the surface level have remained unclear. To address this issue, we therefore characterized the fault structures at five sites (Fig. 2) by a multi-disciplinary approach, including 1) outcrop geological observations along the Dajia River, 2) nine 100–200-m long, near-surface geophysical surveys in the Fengyuan area by electrical resistivity tomography (ERT) techniques, and 3) compilation of shallow borehole data, in order to better determine the location and extend of the surface traces of the Sanyi Fault and the fault geometry in 3-dimensions (3D).

In the following sections, we first present the regional tectonic setting of the fold-and-thrust belt of Taiwan, before zooming in to the local geology of the study area of the southern Sanyi Fault. We then describe briefly the methodology of this study, mainly a combination of geologic investigations, geophysical ERT surveys, and borehole data from the Central Geological Survey (CGS) and Taiwan Area National Expressway Engineering Bureau (TANEEB, also became Freeway Bureau in 2017) open reports (Yen, 2014; Sinotech, 2017). Our results derived a relatively well-constrained zone of fault surface traces with multiple branches. This study better identifies the location of fault surface traces and characterizes the deformation structures and fault architecture in 3D, thus provides a valuable basis for government agencies on defining the 'fault avoidance zone' of the Sanyi Fault in terms of seismic mitigation and city planning. Finally, we discuss the recurrent time of the Sanyi Fault for large earthquakes by incorporating the data from literature.

2. Tectonic and geological setting

Occupying the convergent boundary between the Philippine Sea plate and the Eurasian plate since 5–6 Ma, the fold-and-thrust belt of the Taiwan mountain range represents a tectonically active area of about 20–30 km wide and 300 km long. In the middle part of the Taiwan fold-and-thrust belt, along the Sanyi-Chelungpu Fault system (Fig. 1), the Mio-Pliocene passive margin shallow marine sedimentary sequences are thrust over late Quaternary terrestrial molasse deposits (Tan, 1936; Otuka, 1936; Chang, 1951; Meng, 1963; Tang, 1969; Suppe and Namson, 1979; Hung, 1994; Lin et al., 2000, 2008). The Sanyi Fault generally has a gentle dip-angle of 15–30 degrees. It has accommodated geological vertical throw that varies from 3 to 4 km in the north to 2–3 km in the south, according to the previous studies, including surface investigations (Otuka, 1936; Chang, 1994; Ho and Chen, 2000; Lin et al., 2002), and industrial subsurface surveys of seismic reflection and borehole drilling (Suppe and Namson, 1979; Yang et al., 2007).

At the surface, the footwall of the Sanyi Fault consists primarily of the Quaternary Toukoshan Formation (~1.6–0.5 Ma and nearly one thousand meters thick), which is locally covered by late-Quaternary to Holocene alluvial deposits (several to tens of meters thick) (Fig. 1). On the hanging wall side, the stratigraphic units, from oldest to youngest, include the Tungkeng Formation (~10–5 Ma), the Kueichulin Formation (~5–3 Ma), the Chinshui Shale (~3–2.5 Ma), the Cholan Formation (~2.5–1.6 Ma), the Toukoshan Formation (younger than 1.6 Ma) and alluvial deposits.

In map view (Fig. 1a), the southern Sanyi Fault runs parallel to the northern Chelungpu Fault for about 10–12 km in the Fengyuan area, before terminating toward the south around the city of Taiping. Based on the relatively older rock units on the Sanyi Fault's hanging wall, the Chelungpu Fault can be treated as a relatively younger 'splay fault' to the Sanyi Fault. The geological data including surface and subsurface surveys suggest that the Sanyi fault accommodates larger, long-term total displacement than the Chelungpu Fault, which is responsible for 1999 earthquake and has a recurrent time of 300–500 year (Chen et al., 2004; Wang, 2005; Le Béon et al., 2014), arguing for potential significant seismic risk. To the north, the surface traces of the northern Sanyi Fault closely conforms to the topographic escarpment of dissected hills. South of the Dajia river, however, the southern Sanyi Fault is generally buried by late Quaternary deposits (Fig. 2).

3. Methodology: combination of geological and geophysical surveys

In this study, we conducted geological and geophysical investigations along the possible surface traces of the southern Sanyi Fault. As we mentioned above, the surface traces of the southern Sanyi Fault are mostly buried by the alluvial or fluvial deposits, except the excellent exposure at the Dajia River. As a result, we used the exposure in the Dajia River (Site A, Fig. 2) as a case study site. Geological field investigations as well as geophysical surveys were carried out in the site of the Dajia River, that allowed us to analyze the architecture of the Sanyi Fault at the surface level. The fault-associated deformation structures observed in these outcrops served as the basis to interpret the geophysical imaging data, especially for the sites further south in the alluvial plain.

For the area covered by the alluvial or fluvial deposits, we conducted geophysical ERT imaging investigations at 4 out of 5 sites (Sites A, B, C, and D in Fig. 2). Due to the intensive population development in the urban area, it was quite challenging to find the places amenable to the ERT surveys, resulting in relatively short survey lengths. In total, we produced nine ERT profiles with lengths from 70 m to 160 m. For the field surveys, we adopted the Wenner/Schlumberger array with a separation of sensors of 3–5 m. The location of survey lines is presented as red bars in Fig. 2.

Following the field surveys, resistivity images were derived from the smooth model inversion by using EarthImager 2D software from Advanced Geosciences Inc., which is based on the data weighting from the Gaussian distribution of standard errors. The inversion was carried out to minimize the root mean square (r.m.s.) error between ERT apparent resistivity and response of a resistivity model. The r.m.s. error of the uncertainty of final results was estimated to be less than 10%.

In addition to the ERT data we have incorporated borehole and trenching data archived by the CGS and TANEEB in available open reports (Yen, 2014; Sinotech, 2017). In particular at Site E (the southernmost site), an array of 7 shallow boreholes provided good constraint on identifying a ~ 300 m wide zone with multiple fault branches, which also served as criteria to map the location and extend of the fault. Finally, we have integrated these subsurface constraints with our ERT findings to create a reconstruction of the architecture and structures of the southern Sanyi Fault at shallow levels.

4. Results

4.1. Site A: outcrops in Dajia River

4.1.1. Geological outcrop observations

Site A is the northernmost site, located at the Dajia River (Fig. 2), where good rock exposures crop out on the both banks of the river, as well as the river beds. The outcrops on the northern bank previously have been reported by Lee (1994), indicating the evidence of the deformation structures associated with the Sanyi Fault. We used the clear outcrop relations to guide the locations of ERT surveys that we then used to benchmark our expectations for surveys of the fault where it is blind.

On the northern bank, we observe the shallowly east-dipping sandstone layers (i.e., the late Miocene Kueichulin Formation) are thrust over the flat-lying gravel layers (late Quaternary Toukoshan

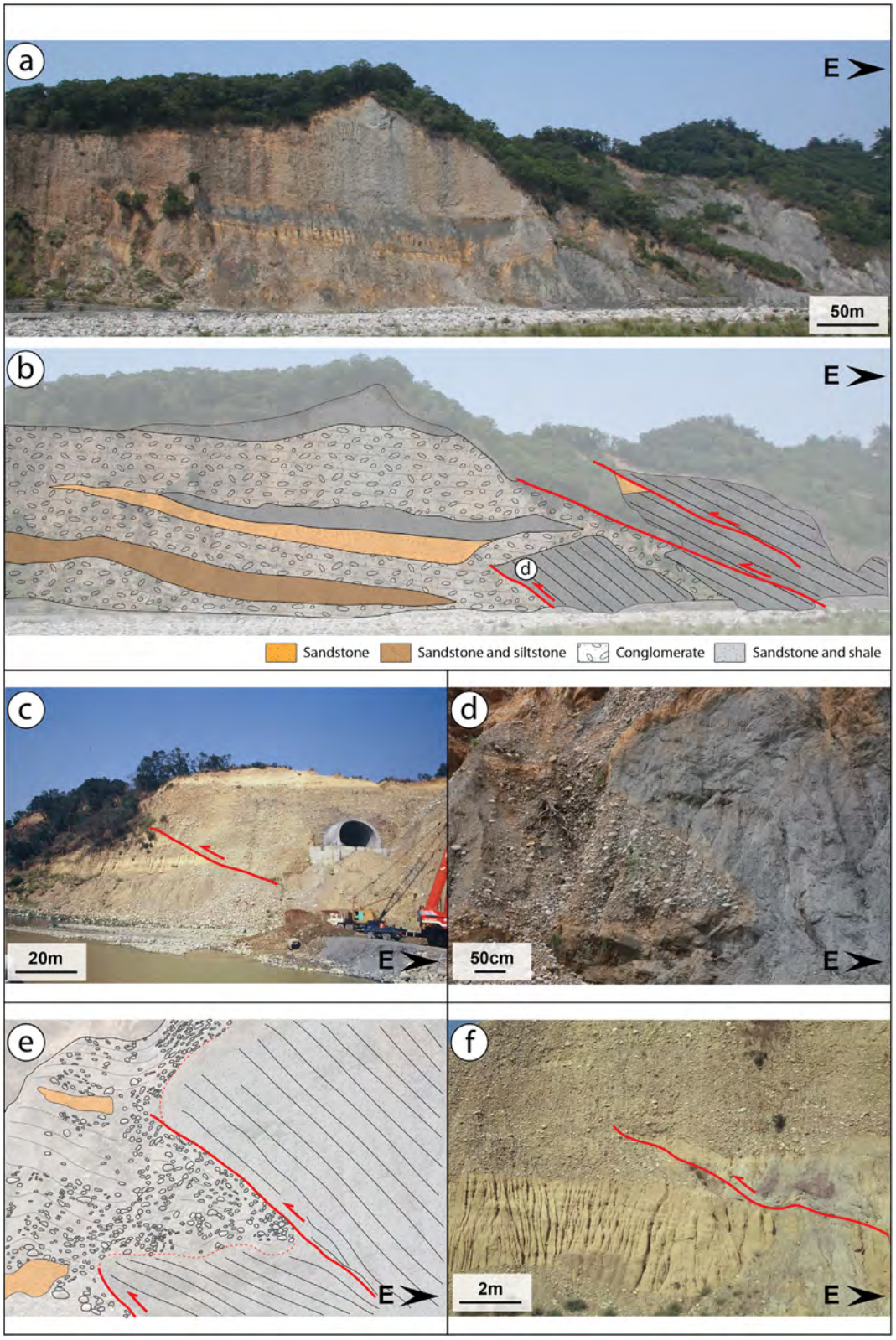

Fig. 3. Photographs of the rock exposure on the north bank of the Dajia River. In this outcrop, the Sanyi Fault is characterized by four major fault branches (three in Fig. 3a, b and one in Fig. 3c) within a distance of ~400 m. Along the primary fault zone, the gently east-dipping Miocene Kueichulin sandstone is overthrust onto the flat-lying Pleistocene Toukoshan conglomerates and the late-Quaternary alluvial deposits. In the conglomerates near the fault, we can also observe subtle folding structures revealed by arrays of pebbles (Fig. 3d, e, and f). The westernmost fault branch occurred within the conglomerates in the footwall of the primary fault zone (Fig. 3c) and it is also located near the major topographic scarp between rugged hills and flat plain to the west.

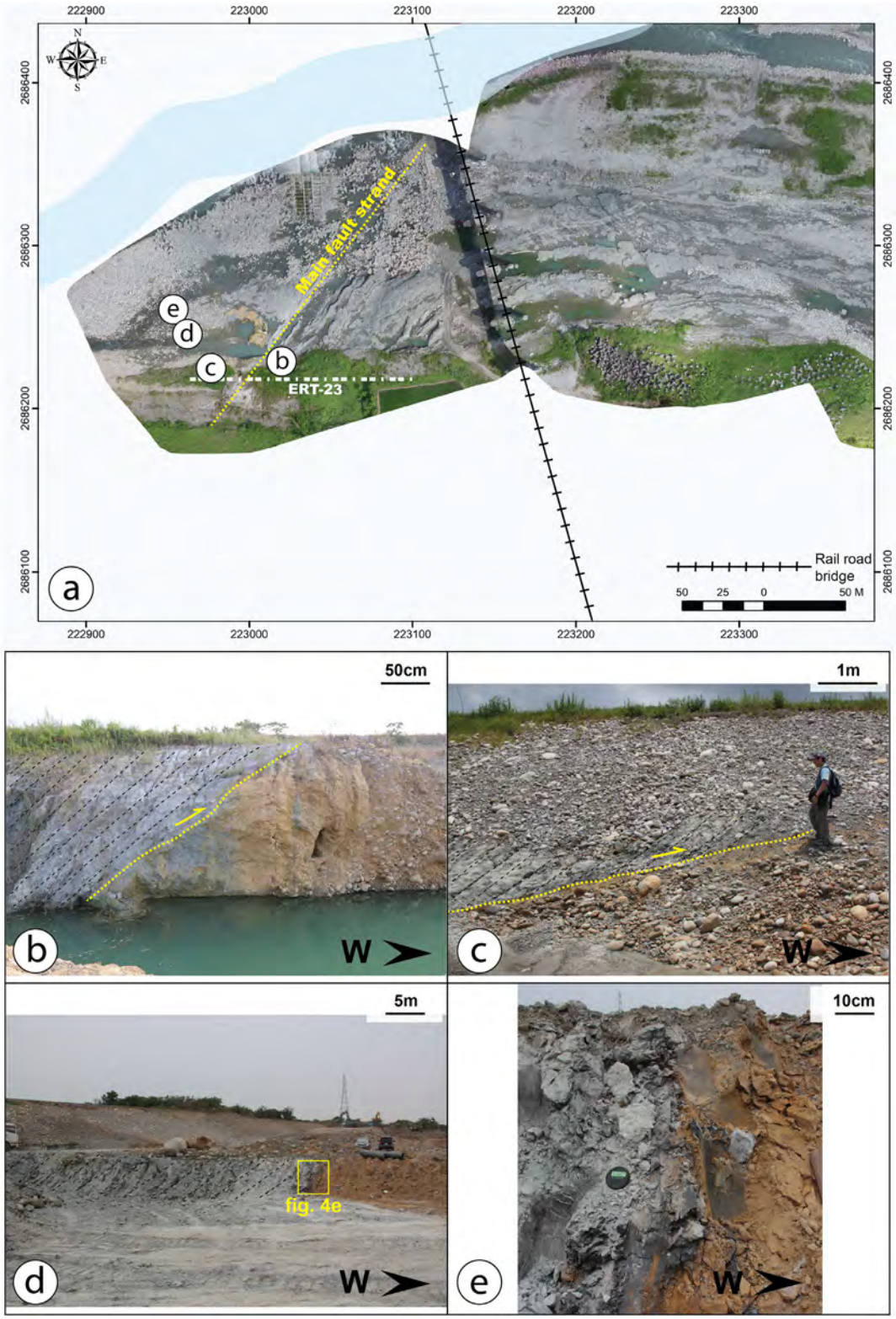

Fig. 4. (a) UAV aerophotograph of the southern bank of the Dajia River. Letters 'b', 'c', 'd' and 'e' indicate the locations of the outcrop photographs on the south bank. A continuous outcrop showing the grayish sandstone (east-dipping, grey dashed lines) thrust onto the yellowish sandstone (b) and gravels (c) at a shallow angle. (d) Photographs of outcrop showing a fault strand along which the grayish sandstone is thrust onto the yellowish conglomerate at an angle of 50–60. (e) Close view of Fig. 4d showing a sharp fault contact marked by clayey fault gouge ~5 cm-thick.

conglomerate) (Fig. 3a and b). This 500–600-m-wide outcrop shows the Sanyi Fault zone consisting of at least four branches (Fig. 3b and c). One fault branch is covered by the flat-lying conglomerate layer (Fig. 3d and e), indicating an earlier fault strand ceased its activity (Fig. 3d). Along this fault branch we observed subtle folding structures within the imbricated gravels, indicating a top-to-the-west sense of movement of the Sanyi Fault (Fig. 3e). The westernmost fault branch cuts across the conglomerate layers near the railway tunnel, and has been described

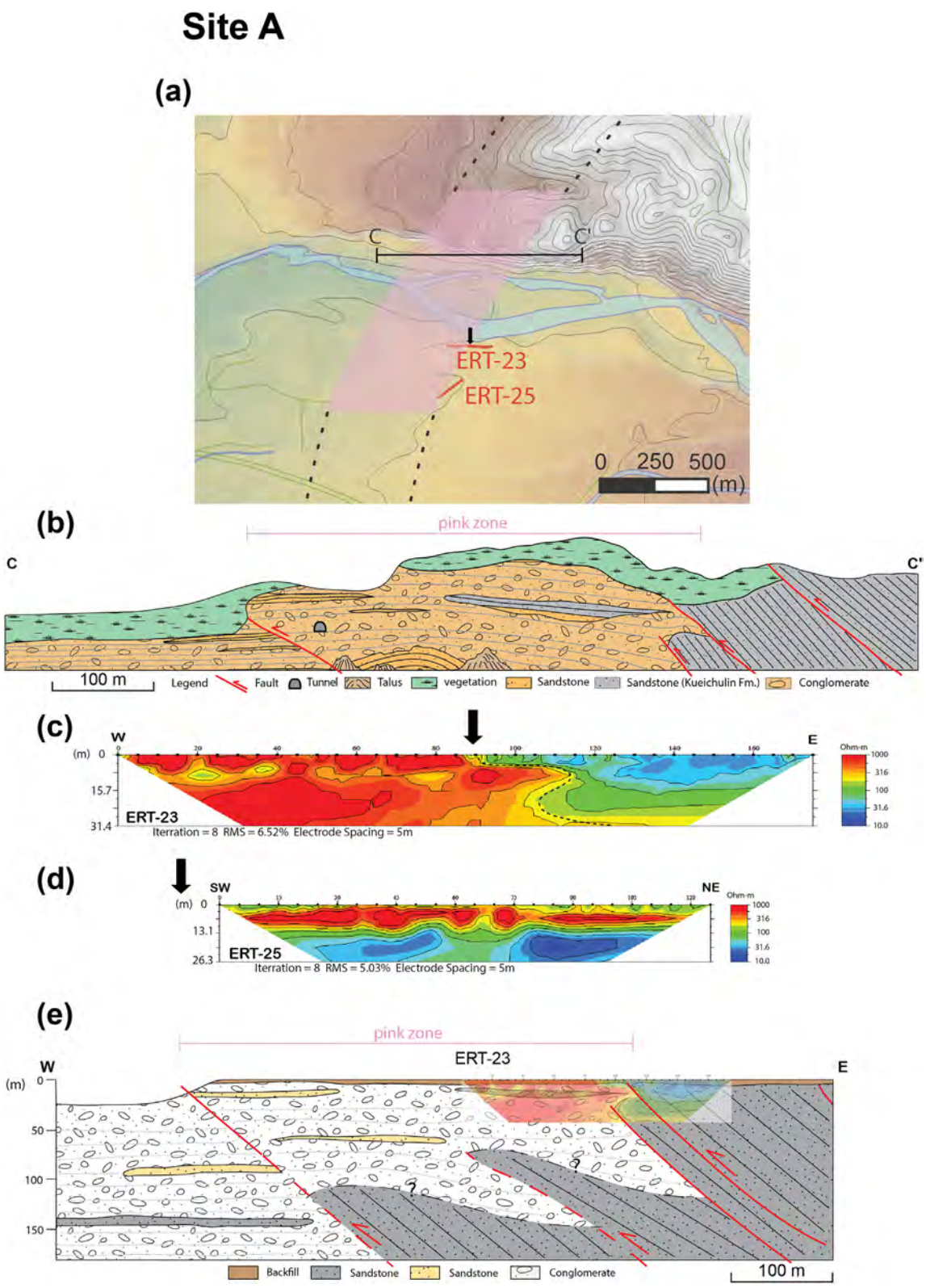

Fig. 5. Results of Site A along the Dajia River. (a) Location map of our geological observations and geophysical ERT survey profiles. The Sanyi Fault surface traces (pink zone) were determined from the outcrop with four branches (Dajia River). (b) Geological profile along the northern bank of the Dajia River, based on the outcrop observations. (c) Results of profile ERT-23. The sharp contrast between high and low resistivities is interpreted as the primary fault zone of the Sanyi Fault. The 'Z' shape resistivity boundary implies a complex fault zone with multiple branches. (d) Result of ERT-25 showing an 8–10 m thick high resistivity layer at the surface, indicating fluvial gravel deposits. The gravels are underlain by a lower resistivity unit, which we interpret as the Kueichulin sandstone. Black arrows show location of the Sanyi Fault trace. (e) Schematic geological cross section at Site A. The Sanyi Fault zone with four major branches is approximately 400 m wide at this site. We interpret that the Kueichulin sandstone is thrust over the conglomerate in the downdip part of the westernmost branch. See the index map in Fig. 2 for the location of the site. (For interpretation of the references to colour in this figure legend, the reader is referred to the web version of this article.)

previously (e.g., Lee, 1994; Lee and Chu, 1998) (Fig. 3c and f). This fault branch is located near the major geomorphic break which separates the rugged hills to the east from the flat fluvial terrace and alluvial deposits to the west.

On the southern bank of the Dajia River (Fig. 4), the exposure is less continuous than on the northern bank. Nevertheless, we found a few pieces of evidence of surface faults at distributed outcrops. At one locality (Fig. 4b), we observed one fault branch (strike/dip: N40E/62S) which separates the east-dipping grayish sandstone from the yellowish gravels. To the west, a second fault branch crops out through the east-dipping grayish sandstone from the likely flat-lying gravels (Fig. 4c). At another locality (Fig. 4d), we found a thrust fault branch (strike/dip: N46E/64S) that puts sandstone of the Kueichulin Formation on top of the yellow unconsolidated gravel/sandstone layers, and that is marked with fault gouge (Fig. 4e). We interpret this is also a multiple fault branch system of the Sanyi Fault on the southern bank.

4.1.2. Geophysical surveys and images

We conducted two ERT field surveys along the southern bank of the Dajia river (Fig. 5a). The 170-m-long ERT-23 profile (Fig. 5c) adjacent to the outcrops along the river edge, shows a sharp resistivity contrast between a high-resistivity rock unit ($>$ 300 Ωm) and a low-resistivity rock unit ($<$ 100 Ωm). We interpret the change in resistivity to mark the primary Sanyi Fault zone, i.e., the high resistivity corresponds to the gravels layers and the low resistivity corresponds to the sandstone layers. The ERT boundary exhibits a *Z*-shape curve across a width of 50–60 m, indicating a rather complex fault zone structure, probably with several fault branches, as seen in the geological outcrops of the northern and southern banks (Fig. 5b).

The second survey is the 120-m-long ERT-25 profile (Fig. 5d), located about 200 m south of the riverbed. This location is characterized by a surface alluvial cover of 8–10 m thick with high resistivity values, which is underlying by the bedrock with lower resistivity values (Fig. 5d). No clear evidence of major fault was observed in the ERT-25 profile. We interpret that the profile lies on the hanging wall of the Sanyi Fault and the primary fault is located further west of this ERT profile.

4.1.3. Synthesis

Combining the geological observations and the ERT geophysical surveys, we reconstruct a geological structural cross section of the southern Sanyi Fault at the shallow level (several tens of meters deep) (Fig. 5e). We interpret a ~ 400-m-wide branching fault system at this site. The primary fault zone, which we define as the Kueichulin sandstone layers thrusted over on the Toukoshan conglomerate layers, is situated near the eastern edge of this ~400 m wide zone (see pink shading in figures). And the western edge of the zone is defined by the westernmost fault branch within the conglomerate layers at the surface level. We tentatively interpret that the Kueichulin sandstone in the hanging wall lies downdip of the westernmost fault branch (Fig. 5e). Note that the westernmost branch follows the major geomorphic scarp.

As a result, in terms of mapping the surface traces of the Sanyi Fault, we propose to use a wide 'fault zone' to represent the surface ruptures zone. As indicated by the outcrops on the northern bank of the Dajia River, the Sanyi Fault is characterized by multiple fault branches, which are distributed across a few hundred meters across strike. We show this zone on our maps as a 'pink zone' of ~400 m wide to cover the extend of the possible multiple fault branches at this site (Fig. 5).

4.2. Site E: Xintian village

This is the southernmost site near the village of Xintian (see location on Fig. 2). Previously at this site the TANEEB drilled a series of boreholes and dug a short trench for paleoseismological study (Fig. 6). We will provide additional age constraints from paleoseismological study in the trench at this site in the section of Discussion. Compiling the TANEEB's borehole data, we adopted a geological cross section from TANEEB's open report at this site (Fig. 6b; Sinotech, 2017). A multiple fault system with three major fault branches represents the general structural architecture at this site. In Fig. 6, we can find that the Kueichulin sandstone crops out in the hanging wall of the easternmost fault branch. The cores from the boreholes showed that at the subsurface level the east-dipping Kueichulin sandstone is thrust onto flat-lying conglomerates along the two other fault branches, although they are covered by the conglomerates and alluvial deposits. The fault zone has a width of about 300 m. It is worth noting that the fault zone is located near a topographic scarp, implying the possibility of recent activity on the Sanyi Fault. This conclusion is in accord with the borehole observations that all three fault branches cut late Quaternary or Holocene alluvial deposits. We also observe that the Chelungpu Fault appears about 400 m to the east of the Sanyi Fault that is in accordance with the observations in the TCDP drilling data.

In summary combining results from Sites A and E, the geological and deformation structures of the Sanyi Fault provide a generally consistent multiple branch fault zone of 300–400 m wide. Conservatively, we thus adopted a ~ 400 m wide zone (pink zone) and applied it to other three sites (Sites B, C, and D) for mapping the possible location and extend of the surface traces.

4.3. Site B: Weishe village

At Site B around the village of Weishe, the Sanyi Fault is covered by alluvial deposits without any clear geomorphic expression. As a result, borehole data and geophysical surveys become critically important for mapping the surface traces of the Sanyi Fault.

In 2015, with support of the CGS, we conducted ERT geophysical surveys around the village of Weishe (Figs. 2 and 7a), based on the projected extension of the Sanyi Fault observed at the site of Dajia River. Our ERT results of profiles ERT-09 (Fig. 7b) and ERT-10 (Fig. 7c) show a zone with sharp gradient in electric resistivity near the eastern end of both profiles. We interpret this ERT contrasting boundary as the primary fault zone of the Sanyi Fault, that separates the conglomerates (high resistivity of $>$ 300 Ωm) to the west and the sandstone layers (lower resistivity of $<$ 100 Ωm) to the east. The results from two other ERT survey lines showed that they are either in the hanging-wall side (ERT-01, Fig. 7d) or in the footwall side (ERT-05, Fig. 7e).

We also incorporated the nearby borehole data from drilling in 2014, reported by CGS. The four boreholes, BH-2A, 2B, 2C, and 2D, however, all appear to be located in the hanging wall of the Sanyi Fault. The cores reveal gently *E*-dipping sandstone layers (Kueichulin Formation) and the overlying alluvial gravel layer of about 8-m thick. Based on the correlation of resistivity to lithology established adjacent to the south bank of the Dajia River, the shallow gravel layers correspond to higher resistivity value ($>$ 300 Ωm in ERT-01) and Kueichulin sandstone corresponds to lower resistivity values ($<$ 100 Ωm in ERT-01).

Combining the above data from boreholes and geophysical surveys and observations of multiple fault branches at Site A and Site E, we suggest that trace of the Sanyi fault in the vicinity of Weishe village could be conservatively mapped as a 400-m-wide zone (pink zone in Fig. 7a and f). We adopt the primary fault zone observed in two ERT profiles (ERT-09 and 10) as the eastern edge of the 400 m wide zone. Based on the regional topographic 20-m DEM, it reveals a NNE-trending geomorphic slope break, although quite subtle, which we tentatively interpret to be sub-parallel to the principal trend of surface traces of the Sanyi Fault.

4.4. Site C: Fengyuan city

About 1–2 km further south near the city limit of Fengyuan, we were able to conduct only one ERT survey line (ERT-20, Fig. 8). It is worth noting that this is an urbanized area and the land is mostly

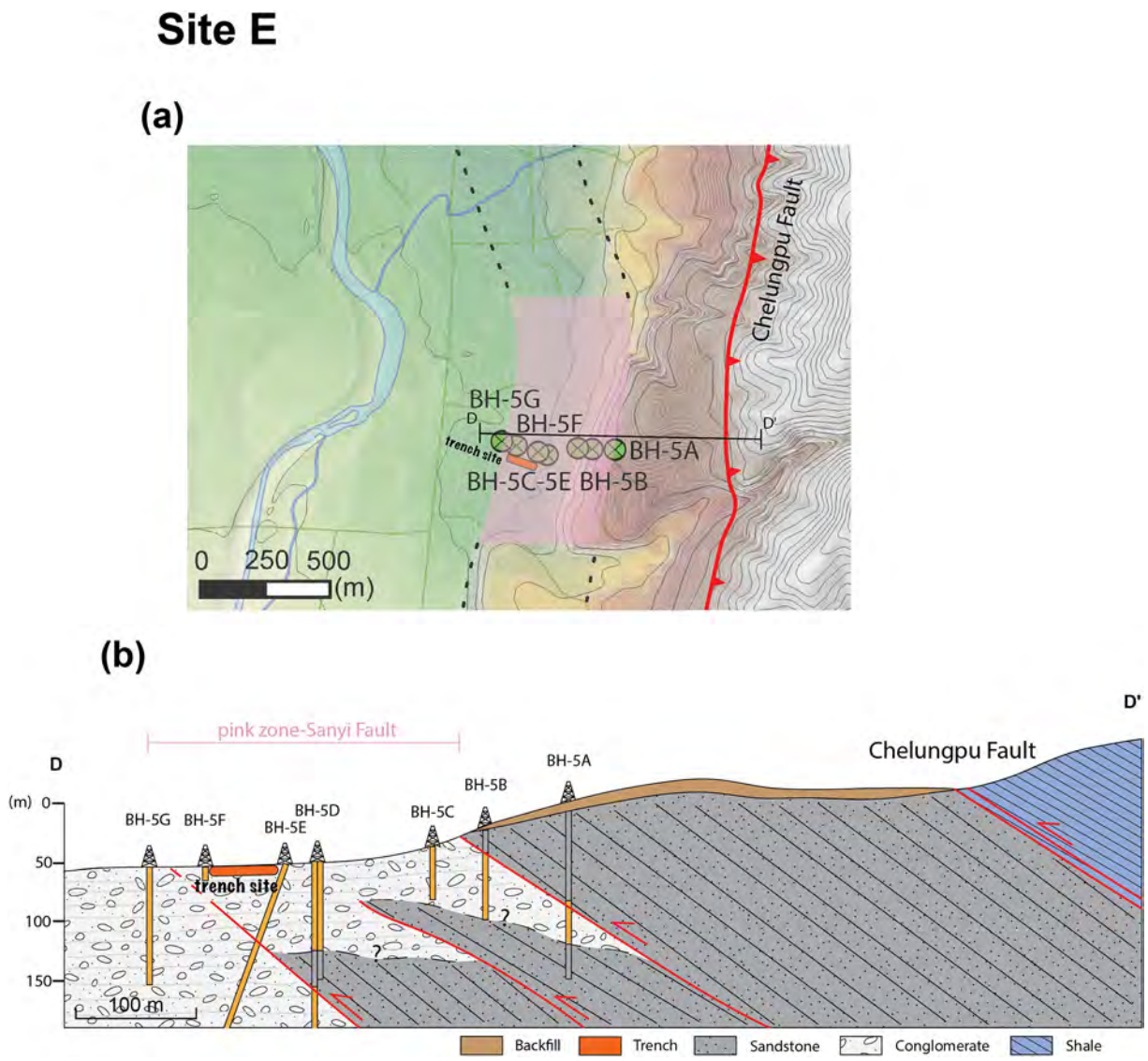

Fig. 6. Results of Site E in Xintian village. (a) Location of 7 boreholes and 1 paleoseismological trench, which have been used to interpret the architecture of the Sanyi Fault, at Site E. (b) Interpreted geological cross section at Site E. At the surface level, the Sanyi Fault zone, which is composed of three major fault branches, is shown as a pink zone with a width of 300 m. It is worth noting the Chelungpu Fault which follows a major topographic scarp is located about 400 m east of the Sanyi Fault at this site. See the index map in Fig. 2 for the location of the site. (For interpretation of the references to colour in this figure legend, the reader is referred to the web version of this article.)

occupied by man-made structures, so appropriate sites for conducting ERT surveys are very limited. Unfortunately, the result of profile ERT-20 did not show clear evidence of major fault within the survey line. High resistivity values dominate the profile indicating that the whole profile is likely located in the gravel and conglomerate layers, that is, on the footwall side of the Sanyi Fault. The ERT profile allows us to identify a 3–4-m-thick surficial alluvial deposits (a lower resistivity of < 100 Ωm), which overlies on the conglomerates of the Toukoshan Formation (a higher resistivity of > 300 Ωm) (Fig. 8b).

Further east, the CGS drilled an array of three geological boreholes (2014–2015, but under a different project) (Fig. 8a), which provided lithological constraints on locating the projected surface trace of the buried Sanyi Fault. In this drilling array, boreholes BH-3A and BH-3C penetrated 3–8 m of gravels/sand (Holocene alluvium) and underlying thick sandstone (late Miocene Kueichulin Fm.) that are considered to be located in the hanging wall of the Sanyi Fault. Borehole BH-3B, in contrast, penetrated exclusively gravels/conglomerates from 0 to 50 m of depth, thus is considered to be located on the footwall side. Based on the above borehole data, we infer that the surface traces of the Sanyi Fault occur between the BH-3B and BH-3C (Fig. 8c).

Like the other sites, we suggest ~400-m-wide zone (pink zone in Fig. 8a) to represent the possible location and extend of the multiple surface trace. We take the primary fault zone, which is situated between the boreholes BH-3B and 3C, near the eastern edge of this zone. For the map view trend of the Sanyi Fault at this site, we infer that the trace coincides with the subtle topographic slope break exhibited by of the 20-M DEM.

4.5. Site D: Fengtian village (south of Fengyuan city)

Near the village of Fengtian, about 2 km south of the city of Fengyuan, we conducted two ERT survey lines (ERT-14 and ERT-16) (Fig. 9a). Profile ERT-14 reveals a dominant high resistivity that indicates the survey line is situated in the thick Toukoshan conglomerates of the footwall (Fig. 9b). As for the results from ERT-16, a clear change of resistivity, from high resistivity (conglomerate) to the northwest to lower resistivity (sandstone) to the southeast, showing a typical ERT feature for the Sanyi Fault (Fig. 9c). We also note there exists an

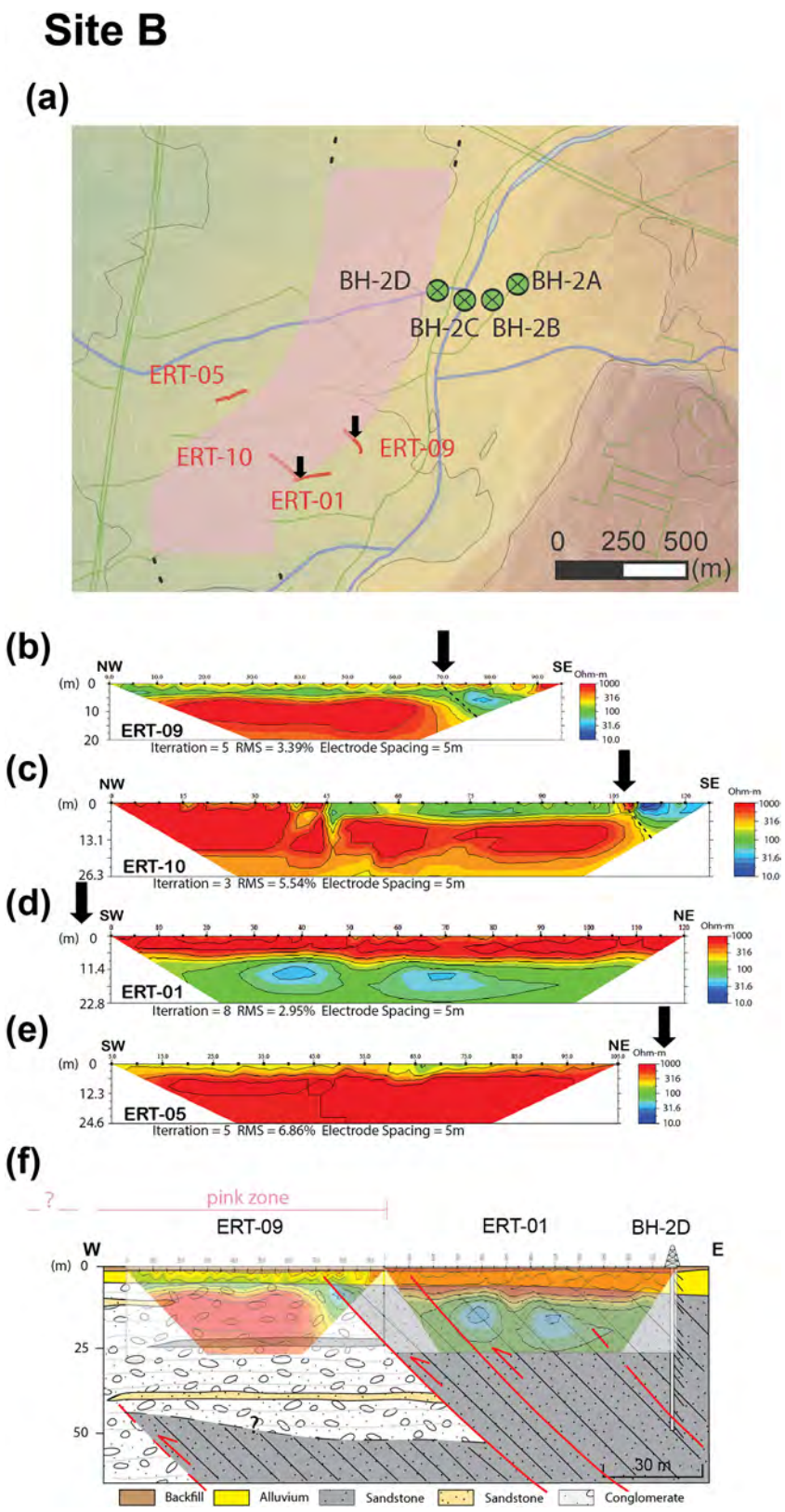

Fig. 7. Results of Site B in Weishe village. (a) Location map of 4 boreholes and 4 ERT profiles providing the key data for mapping the surface traces of the Sanyi Fault (pink zone). (b) and (c) Two ERT profiles, ERT-09 and ERT-10 revealed evidence of fault (black arrows) with contrast between high resistivity (conglomerate) and low resistivity (sandstone). (d) Electrical profile ERT-01 showing 8–10 m surface high resistivity layers (alluvial) and underlying low resistivity unit (sandstone). We interpret the ERT-01 is located on the hanging wall side. (e) Electrical profile ERT-05 showing 3–6 m moderate resistivity layers (alluvial deposits) and underlying high resistivity unit (conglomerate). We interpret the ERT-05 is located on the footwall side. Note that the shallow boreholes BH-2A, 2B, 2C and 2D all appear to be located in the hanging wall. (f) Schematic geological cross section at Site B. We interpret an architecture of multiple fault branches with a width of about 400 m, which we correlate with the observations of Sites A and E. See the index map in Fig. 2 for the location of the site. (For interpretation of the references to colour in this figure legend, the reader is referred to the web version of this article.)

unconsolidated cover of about 10–15 m thick, showing moderate resistivity values (~50–200 Ωm).

Again, we incorporated data from four nearby geological boreholes drilled by CGS's project. Boreholes BH-4A and 4B, which penetrated 14–18 m of unconsolidated gravel/sand layers (alluvial deposits) and underlying sandstones (the late Miocene Kueichulin Fm.), are considered to be in the hanging wall of the Sanyi Fault. To the west, boreholes BH-4C and BH-4D, encountered exclusively of gravel layers from 0 to 50 m, thus we suggest they are located in the footwall of the Sanyi Fault. We interpret that the projected surface trace of the buried Sanyi Fault is located between boreholes BH-4B and BH-4D.

As a result, we conservatively place the eastern edge of the surface

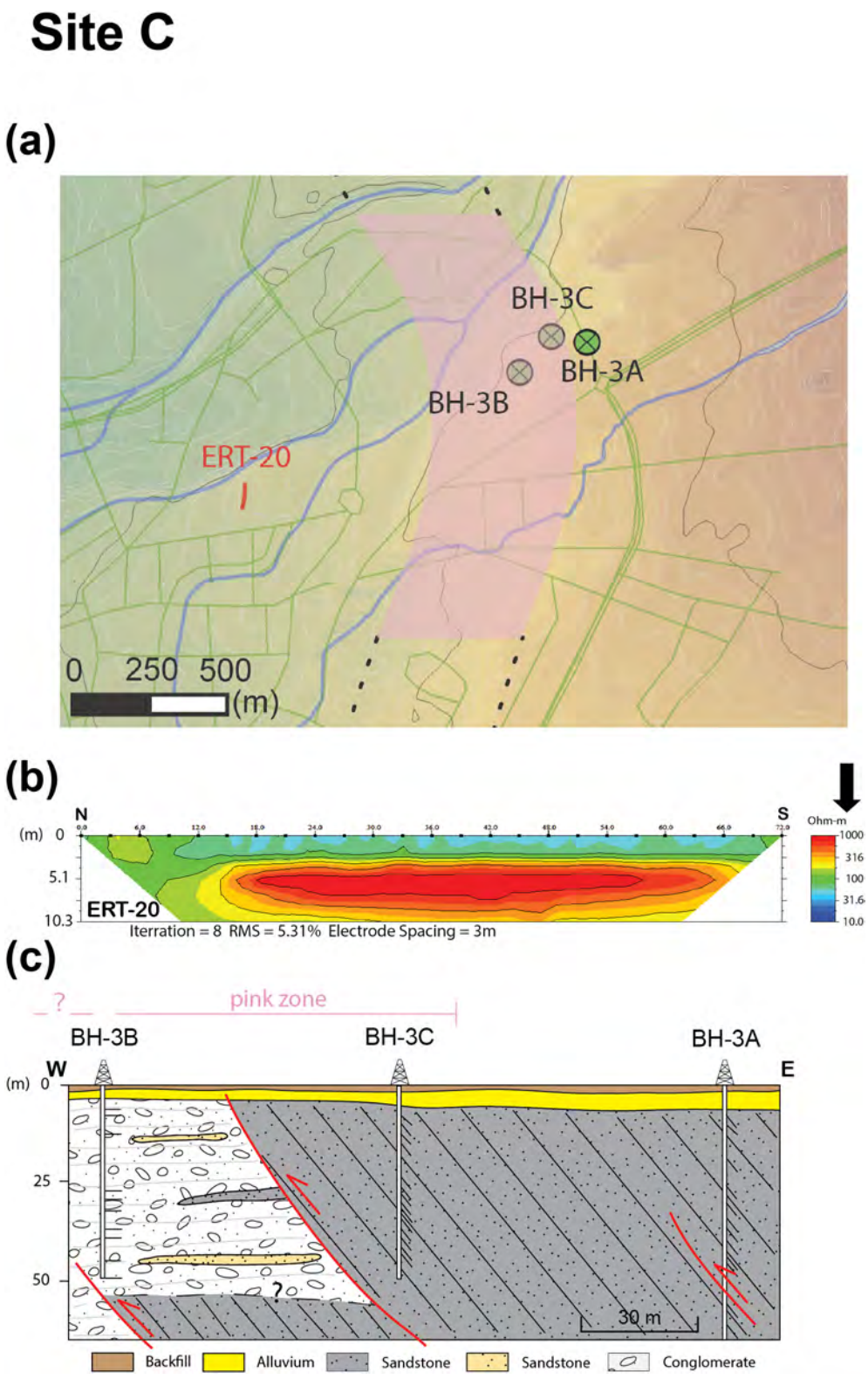

Fig. 8. Results of Site C in Fengyuan city. (a) Location map showing 3 boreholes and 1 ERT profile were integrated into our analyses at this site. (b) Electrical imaging profile ERT-20 showing 3–4 m surface layer with moderate resistivity (alluvial deposits) and underlying unit with high resistivity (conglomerate). We interpret the ERT-20 line is situated in the footwall. (c) Schematic geological and structural cross section at Site C. The boreholes BH-3A and 3C indicate the cores are composed of the Kueichulin sandstone with alluvial deposits in the upper few meters. We attribute the BH-3A and BH-3C are located in the hanging wall. On the other side, the cores of BH-3B are exclusively composed of gravels, indicating the borehole is in the footwall. We thus use the above constraints to provide a ~ 400 m wide fault zone (pink zone) to represent the location of the Sanyi Fault surface traces. See more detailed explanation in the main text. See the index map in Fig. 2 for the location of the site. (For interpretation of the references to colour in this figure legend, the reader is referred to the web version of this article.)

rupture zone between boreholes BH-4B and BH-4D and draw a draw a ~ 400-m-wide fault zone, expanded relative to the other sides (Fig. 9a and d).

4.6. Summary

Combining the results at five sites, we provide a map (Fig. 10) synthesizing the surface traces of the southern Sanyi Fault with a 400 m wide pink zone in the alluvial plain around the city of Fengyuan. We connected the pink zones, which represent the location and extend of the surface multiple fault branches at each five sites, to form a narrow band. We can observe that this narrow band appears to follow roughly the topographic contour lines, although there does not reveal sharp geomorphic scarp in the middle part of the area among Sites B, C and D which is covered by Holocene alluvial deposits. This relatively subtle step in topography suggest recent activity of the southern Sanyi Fault,

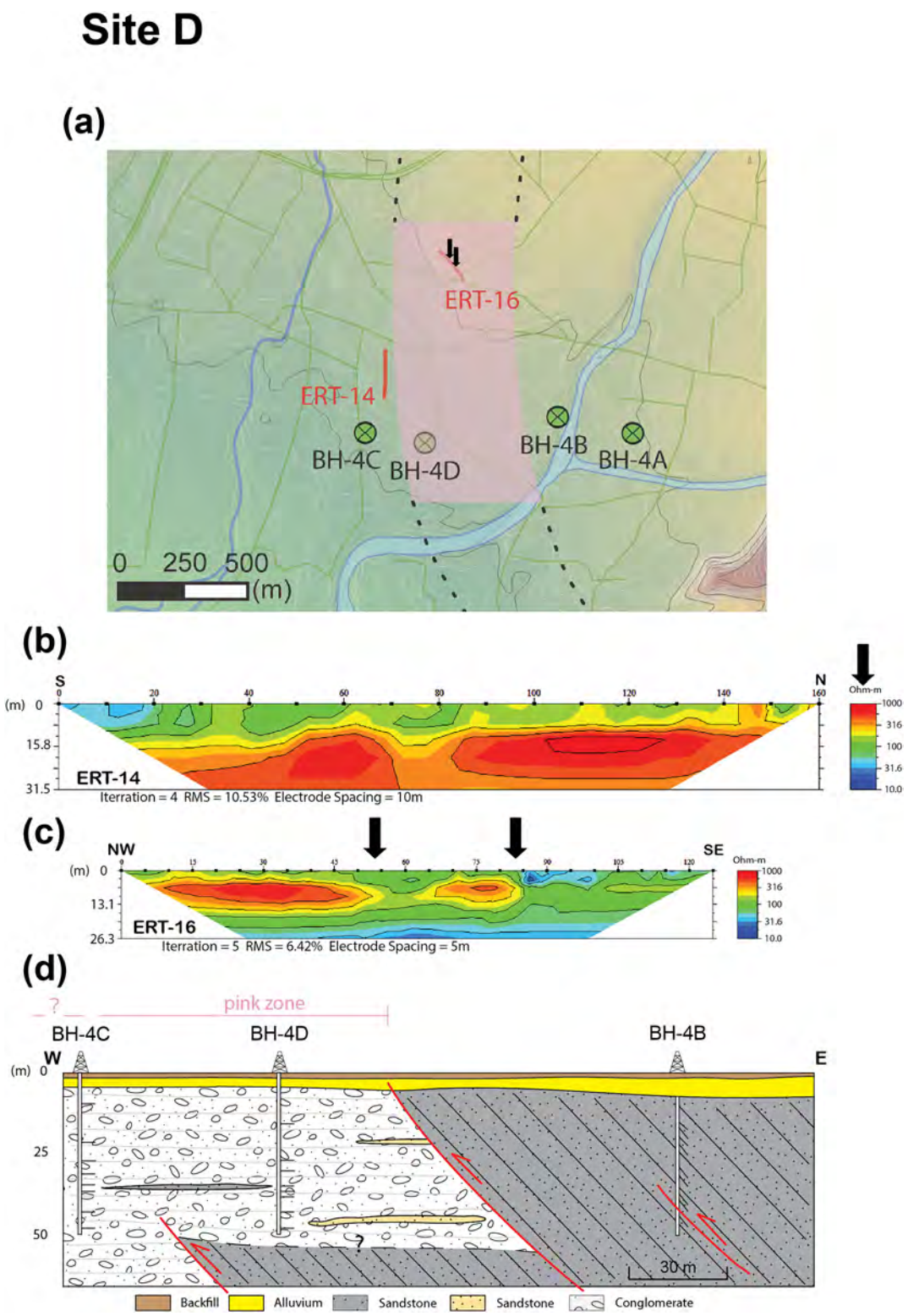

Fig. 9. Results of Site D in Fengtian village. (a) Location map of Site D showing an array of 4 boreholes and 2 ERT profiles used to reconstruct the architecture of the Sanyi Fault. (b) Electrical imaging profile ERT-14, showing conglomerate (high resistivity) and uppermost alluvial deposits (moderate resistivity). The ERT-14 is interpreted to lie in the footwall. (c) Electrical imaging profile ERT-16 showing high resistivity in the west and low resistivity in the east with a subtle, diffuse change of resistivity. We tend to interpret two possible fault branches (black arrows) within this diffuse zone. (d) Schematic geological and structural cross section at Site D. The main lithological boundary (the primary fault) is clearly located in-between BH-4B (*E*-dipping sandstone) in the hanging wall and BH-4D (flat-lying conglomerate) in the footwall. The possible Sanyi Fault surface traces (pink zone) was set to be an approximately 400 m wide zone to cover the primary fault zone and extending toward the footwall. More detailed explanation can be found in the main text. See the index map in Fig. 2 for the location of the site. (For interpretation of the references to colour in this figure legend, the reader is referred to the web version of this article.)

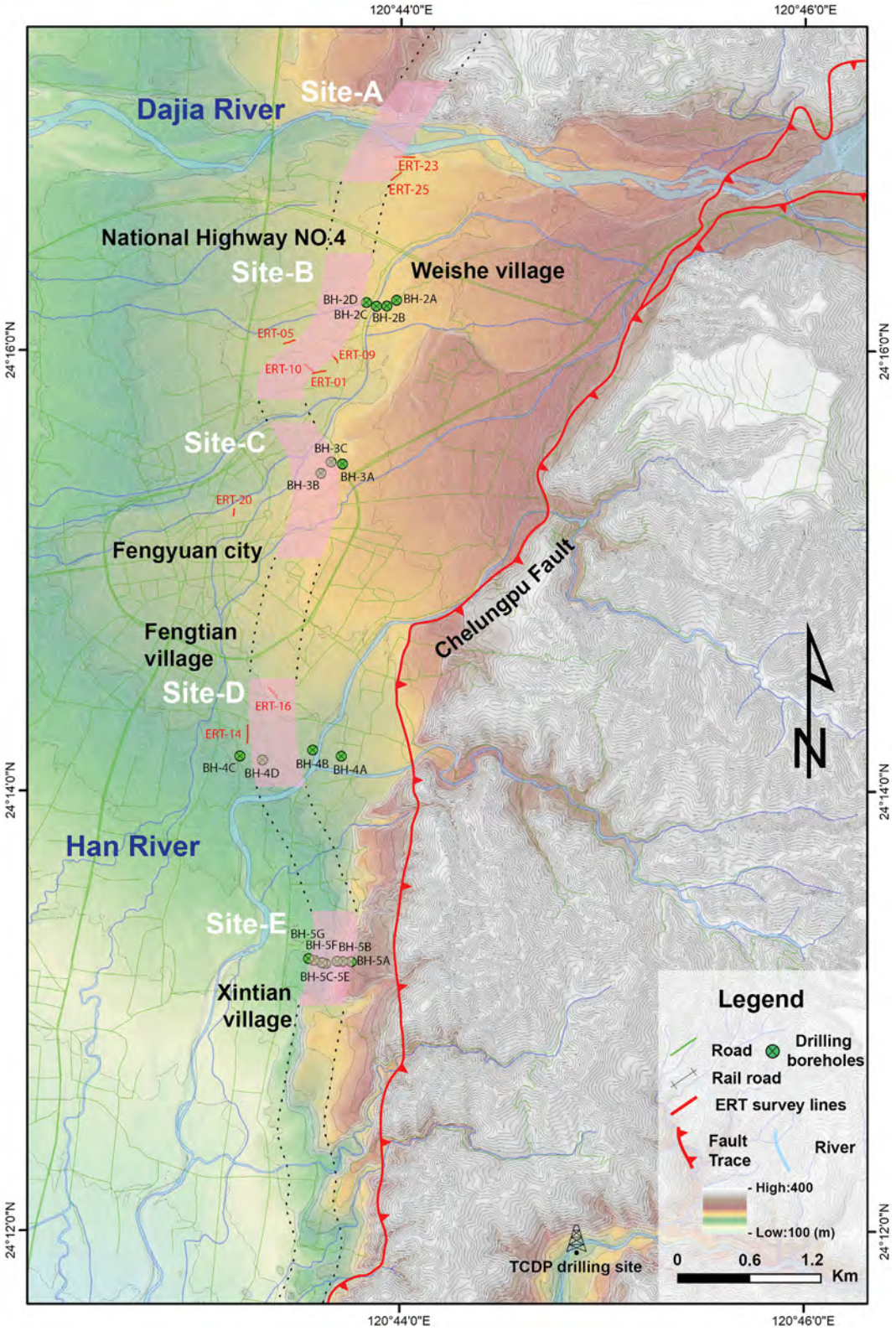

Fig. 10. Map of inferred location of the surface traces of the southern Sanyi Fault. We connected the pink zones determined at each five sites to form a ~ 400-m-wide strip. We can find that our inferred fault zone of the southern Sanyi Fault is in a relatively good agreement with the local topography (20-m DEM). The fault zone generally follows the geomorphic 'scarp', although subtle, in the alluvial deposits. (For interpretation of the references to colour in this figure legend, the reader is referred to the web version of this article.)

possibly associated with significant earthquakes during the Holocene time.

5. Discussion

5.1. Relationship between the Sanyi and Chelungpu Faults

The overlapping configuration at the junction of the Sanyi-Chelungpu Fault system has been noted in previous studies (e.g., Hung and Wiltschko, 1993; Wang et al., 2000, 2002; Hung and Suppe, 2000; Yue et al., 2005; Lee and Chan, 2007). The southern Sanyi Fault runs sub-parallel to the northern Chelungpu Fault for about 10–12 km before the two merged near the city of Taiping. While showing the same north-south striking fault traces, there are different geological formations offset within the Sanyi-Chelungpu Fault system. A larger stratigraphic throw is accommodated by the Sanyi Fault with late Miocene Dongkeng Fm. to the early Pliocene Kueichlun Fm. overthrust onto the late Quaternary Toukoshan Fm. A smaller stratigraphic offset is accommodated by the Chelungpu Fault with late Pliocene Cholan Fm. and Chinshui shale overthrust on the Pleistocene-Holocene Toukoshan Formation and/or the Holocene alluvial deposits. As noted above, the TCDP also interpreted a structural profile across the Dakeng well, in which the Sanyi Fault zone is about 400 m deeper than the Chelungpu Fault zone (1300 vs. 1710 m deep) (Hung et al., 2007). From a broader point of view, the Sanyi Fault has been developing a new thrust fault (or a splay fault) in the younger formations in its hanging wall, thus forming the footwall of the Chelungpu Fault. The Chelungpu Fault eventually formed a thrust fault system to the east and to the south of the Sanyi Fault, as the progressive deformation migrating from north to south in the foothills of the Taiwan mountain belt (Suppe, 1984).

5.2. Age controls of the last event(s) of the Sanyi Fault

Age constraints on the long-term activity (e.g., late-Quaternary slip rate or uplift rate) as well as the short-term activity (i.e., the past earthquake events) of the Sanyi Fault are discussed in this section.

In the northern part of the Sanyi Fault, there is no geological age data in the literature. In the southern part of the Sanyi Fault, where the Chelungpu Fault truncates in the hanging wall of the Sanyi Fault, we compiled the OSL dating results in the Pleistocene Hsin-She uplift river terraces along the Dajia river for which Le Béon et al. (2014) showed depositional ages between 30 and 10 ka. They attributed these uplift terraces to the backfolding of the Chelungpu Fault and estimated a long-term slip rate of 17–18 mm/yr for the Chelungpu Fault. At this point, without further data, it is difficult to determine whether the Sanyi Fault, which lies below the Chelungpu Fault, played a role, and how much, on the uplift Hsin-She terraces.

Near the southern end of the Sanyi Fault at the study Site E in the trench excavated by TANEEB, three paleo-earthquake events (or tilting/folding events) were derived, with the carbon-14 dating ages of 4490–5710 BP, 3400–3720 BP, and after 1860 BP (Sinotech, 2017). Although the number of age constraints is limited, the results suggest that the Sanyi Fault should be considered as an active fault with a recurrent period of large earthquake at the millennium year scale. This is 3–4 times longer than the general recurrent time for its southern neighboring thrust, the Chelungpu Fault, which was estimated about 300–400 years on average in the past few thousands of years (Chen et al., 2004; Wang, 2005; Le Béon et al., 2014). Furthermore, the decade-long geodetic data indicated that the fault is likely locked, revealed by a few mm/yr of horizontal velocity difference across the Sanyi Fault (Central Geological Survey CGS, 2018). However, it is still worth taking consideration on the potential seismic hazards inducing by the Sanyi Fault, particularly for city planning and for defining the fault avoidance zone.

6. Conclusions

We mapped a ~ 400 m wide zone of surface traces of the Sanyi Fault where it runs subparallel and immediately west of the northern Chelungpu Fault from Dajia river to Taiping city. In total we provide constraints for the position of the fault for a distance of 12 km across the alluvial plain near the city of Fengyuan in the western foothills of Taiwan. We make the following conclusions.

1) Whereas along the primary fault zone, the Miocene Kueichulin Formation is thrust over the late-Quaternary Toukoshan Formation, we find that the southern Sanyi Fault includes several branches which are distributed about 400 m wide at the near surface level. Among the five surveys sites, the multiple fault branches in the shallow subsurface (i.e., tens of meters) can be calibrated by the ERT data against the outcrop investigations and the arrayed boreholes analyses.
2) The ERT surveys revealed obvious contrasts in resistivity with low resistivity (< 100 Ωm) on the hanging-wall Miocene sandstone and high resistivity (> 300Ωm) on the footwall Quaternary conglomerates.
3) Combining our geological and geophysical results, we provide a map with a ~ 400-m-wide zone to exhibit the location of the surface traces of the southern Sanyi Fault and its possible width of multiple surface fault strands. This map would provide a basis for further establishing the official surface fault avoidance zone in terms of seismic hazard mitigation.
4) Judging from the geochronological data in the literature, the southern Sanyi Fault shows a recurrence interval of about thousand years scale with the surface folding/tilting in the young Holocene deposits. The earthquake hazards thus should require alert and the city planning in the Fengyuan area needs to take the active Sanyi Fault into account.

Acknowledgment

We appreciate many constructive comments and suggestions from two reviewers (Tim Byrne and one anonymous) and the Editor Janusz Wasowski, that substantially improved the manuscript. The authors would like to thank Prof. Wen-Jeng Huang for providing the UAV picture and the CGS for financially supporting this research under Contract No. 104-5226904000-07-01. This research was also supported by the Ministry of Science and Technology (MOST) of Taiwan (grants MOST 107-2116-M-001 -026 -MY3). This is a contribution of Institute of Earth Sciences, Academia Sinica, IESAS-2380.

Credit author statement

We outline all authors' individual contributions as follows:

Gong-Ruei Ho: Conceptualization, Data curation, Formal analysis, Investigation, Visualization, Writing – original draft, Writing – review & editing.

Ping-Yu Chang: Conceptualization, Data curation, Formal analysis, Funding, acquisition, Investigation, Methodology, Project administration, Resources, Supervision, Validation.

Jian-Cheng Lee: Conceptualization, Formal analysis, Funding acquisition, Investigation, Methodology, Project administration, Resources, Supervision, Validation, Writing – original draft, Writing – review & editing.

Jonathan C. Lewis: Validation, Writing – review & editing.

Po-Tsun Chen: Data curation, Investigation.

Han-Lun Hsu: Data curation, Investigation.

Declaration of Competing Interest

None.

References

Angelier, J., Barrier, E., Chu, H.T., 1986. Plate collision and paleostress trajectories in a fold–thrust belt: the foothills of Taiwan. Tectonophysics 125, 161–178. https://doi.org/10.1016/0040-1951(86)90012-0.

Chang, H.C., 1994. Geologic map and explanatory text of Taiwan 17 Tachia. In: Geological Map of Taiwan Scale 1:50,000. Taiwan, Central Geological Survey, Ministry of Economic Affairs.

Central Geological Survey (CGS), 2018. Observation of Fault Activity (IV): Integrated Monitoring of Active Faults and Earthquake Probabilities Analysis (in Chinese). Central Geological Survey 290 pp.

Chang, L.S., 1951. The "Sansa overthrust" and the related geologic structures. Bulletin of the Geological Survey of Taiwan 3, 13–18.

Chen, W.S., Erh, C.H., Chen, M.M., Yang, C.C., Chang, E.S., Liu, T.K., Horng, C.S., Shea, K.S., Yeh, M.G., Wu, J.C., Ko, C.T., Lin, C.C., Huang, N.W., 2000a. The evolution of foreland basins in the western Taiwan: evidence from the Plio-Pleistocene sequences. Cent. Geol. Surv. Bull. 13, 137–156.

Chen, W.S., Chen, Y.G., Liu, T.K., Huang, N.W., Lin, C.C., Sung, S.H., Lee, K.J., 2000b. Characteristics of the Chi-Chi earthquake ruptures. Spec. Publ. Cent. Geol. Surv. 12, 139–154.

Chen, Y.G., Chen, W.S., Lee, J.C., Lee, Y.H., Lee, C.T., Chang, H.C., Lo, C.H., 2001a. Surface rupture of 1999 Chi-Chi earthquake yields insights on active tectonics of Central Taiwan. Bull. Seismol. Soc. Am. 91 (5), 977–985. https://doi.org/10.1785/0120000721.

Chen, W.S., Huang, B.S., Chen, Y.G., Lee, Y.H., Yang, C.N., Lo, C.H., Chang, H.C., Sung, Q.C., Huang, N.W., Lin, C.C., Sung, S.H., Lee, K.J., 2001b. 1999 Chi-Chi earthquake: a case study on the role of thrust-ramp structures for generating earthquakes. Bull. Seismol. Soc. Am. 91 (5), 986–994. https://doi.org/10.1785/0120000731.

Chen, W.S., Chen, Y.G., Shih, R.C., Liu, T.K., Huang, N.W., Lin, C.C., Sung, S.H., Lee, K.J., 2003. Thrust-related river terrace development in relation to the 1999 Chi-Chi earthquake rupture, Western Foothills, Central Taiwan. J. Asian Earth Sci. 21 (5), 473–480. https://doi.org/10.1016/S1367-9120(02)00072-X.

Chen, W.S., Lee, K.J., Lee, L.S., Ponti, D.J., Prentice, C., Chen, Y.G., Chang, H.C., Lee, Y.H., 2004. Paleoseismology of the Chelungpu fault during the past 1900 years. Quat. Int. 115–116, 167–170. https://doi.org/10.1016/S1040-6182(03)00105-8.

Chinese Petroleum Corporation (CPC), 1974. The Geological Map of Miaoli. Taiwan Petroleum Exploration Division Publication. Chinese Petroleum Corporation, Taiwan, ROC (scale 1:100,000).

Chinese Petroleum Corporation (CPC), 1982. The Geological Map of Taichung. Taiwan Petroleum Exploration Division Publication. Chinese Petroleum Corporation, Taiwan, ROC (scale 1:100,000).

Dadson, S.J., Hovius, N., Chen, H., Dade, W.B., Hsieh, M.L., Willett, S.D., Hu, J.C., Horng, M.J., Chen, M.C., Stark, C.P., Lague, D., Lin, J.C., 2003. Links between erosion, runoff variability and seismicity in the Taiwan orogen. Nature 426, 648–651.

Duffy, B., Campbell, J., Finnemore, M., Gomez, C., 2014. Defining fault avoidance zones and associated geotechnical properties using MASW: a case study on the Springfield Fault, New Zealand. Eng. Geol. 183, 216–229. https://doi.org/10.1016/j.enggeo.2014.10.017.

Guerrieri, L., Blumetti, A.M., Comerci, V., Di Manna, P., Michetti, A.M., Vittori, E., Serva, L., 2015. Surface Faulting Hazard in Italy: towards a first assessment based on the ITHACA database. Eng. Geol. Society and Territory 5, 1021–1025. https://doi.org/10.1007/978-3-319-09048-1_195.

Ho, C.S., 1976. Foothill tectonics of Taiwan. Bulletin of the Geological Survey of Taiwan 25, 9–28.

Ho, H.C., Chen, M.M., 2000. Geologic map and explanatory text of Taiwan 24 Taichung. In: Geological Map of Taiwan Scale 1:50,000, Central Geological Survey, Ministry of Economic Affairs, Taiwan.

Hung, J.H., 1994. Analysis of deformation fabrics in the Sani thrust sheet and the Chuhuangkeng anticline of western Taiwan. Petroleum Geology of Taiwan 29, 105–126.

Hung, J.H., Suppe, J., 2000. Subsurface geometry of the Chelungpu fault and surface deformation style. Inter. Workshop Ann. Commun. Chi-Chi Earthquake 1, 133–144.

Hung, J.H., Wiltschko, D.V., 1993. Structure and kinematics of arcuate thrust faults in the Miaoli–Cholan area of western Taiwan. Petrol. Geol. Taiwan 28, 59–96.

Hung, J.H., Wu, Y.H., Yeh, E.C., Wu, J.C., 2007. Subsurface structure, physical properties, and fault zone characteristics in the scientific drill holes of Taiwan Chelungpu-fault Drilling Project. Terr. Atmos. Ocean. Sci. 18 (2), 271–293. https://doi.org/10.3319/TAO.2007.18.2.271(TCDP).

Hung, J.H., Ma, K.F., Wang, C.Y., Ito, H., Lin, W.R., Yeh, E.C., 2009. Subsurface structure, physical properties, fault-zone characteristics and stress state in scientific drill holes of Taiwan Chelungpu Fault Drilling Project. Tectonophysics 466 (3), 307–321. https://doi.org/10.1016/j.tecto.2007.11.014.

Juang, C.H., Carranza-Torres, C.M., Crosta, G., Dong, J.J., Gokceoglu, C., Jibson, R.W., Shakoor, A., Tang, H., Van Asch, T.W., Wasowski, J., 2016. Engineering geology-A fifty year perspective. Eng. Geol. 201, 67–70. https://doi.org/10.1016/j.enggeo.2015.12.020.

Kao, H., Chen, W.P., 2000. The Chi-Chi Earthquake Sequence: active, Out-of-Sequence Thrust Faulting in Taiwan. Science 288 (5475), 2346–2349. https://science.sciencemag.org/content/288/5475/2346.

Kim, K.Y., Kim, D.H., Lee, S.Y., 2008. Near-surface geophysical studies in the Ulsan Fault Zone of Korea. Explor. Geophys. 39 (1), 78–84. https://doi.org/10.1071/EG08008.

Kim, Y.S., Kihm, J.H., Jin, K., 2011. Interpretation of the rupture history of a low slip-rate active fault by analysis of progressive displacement accumulation: an example from the Quaternary Eupcheon Fault, SE Korea. J. Geol. Soc. 168 (1), 273–288.

Lai, K.Y., Chen, Y.G., Hung, J.H., Suppe, J., Yue, L.F., Chen, Y.W., 2006. Surface deformation related to kink-folding above an active fault: evidence from geomorphic features and co-seismic slips. Quat. Int. 147 (1), 44–54. https://doi.org/10.1016/j.quaint.2005.09.005.

Lee, H., Woo, H.D., Chun, H.J., Im, C.B., 2014. Geological safety evaluation and monitoring of nuclear facility Sites in South Korea. The Journal of Engineering Geology 24 (4), 609–613.

Lee, J.C., Chan, Y.C., 2007. Structure of the 1999 Chi-Chi earthquake rupture and interaction of thrust faults in the active fold belt of western Taiwan. J. Asian Earth Sci. 31, 226–239. https://doi.org/10.1016/j.jseaes.2006.07.024.

Lee, J.C., Chu, H.T., 1998. Field guidebook of pre-conference field trip - Collision Tectonics in Taiwan. Western Pacific Geophysics Meeting 146pp.

Lee, J.C., Chu, H.T., Angelier, J., Chan, Y.C., Hu, J.C., Lu, C.Y., Rau, R.J., 2002. Geometry and structure of northern surface ruptures of the 1999 Mw = 7.6 Chi-Chi, Taiwan earthquake: influence from inherited fold belt structures. J. Struct. Geol. 24 (1), 173–192. https://doi.org/10.1016/S0191-8141(01)00056-6.

Le Béon, M., Suppe, M.J., Jaiswal, M.K., Chen, Y.G., Ustaszewski, M.E., 2014. Deciphering cumulative fault slip vectors from fold scarps: Relationships between long-term and coseismic deformations in Central Western Taiwan. J. Geophys. Res. Solid Earth 119, 5943–5978. https://doi.org/10.1002/2013JB010794.

Lee, J.F., 1994. Sani Fault and their neotectonic significance. Ti-Chih 14 (1), 73–96.

Lin, C.W., Chang, H.C., Lu, S.T., Shih, T.S., 2000. An introduction to the active faults of Taiwan [with explanatory text of the active fault map of Taiwan, scale 1:500,000]. Special Publication of the Central Geological Survey 13, 49–60.

Lin, C.W., Shih, R.C., Lin, Y.H., Chen, W.S., 2002. Structural characteristics of the Chelungpu fault zone in the Taichung area, Central Taiwan. Western Pacific Earth Sciences 2 (4), 411–426.

Lin, C.W., Lu, S.T., Shih, T.S., Lin, W.H., Liu, Y.C., Chen, P.T., 2008. The Sanyi Fault. Special Publication of the Central Geological Survey 21, 21–32.

Meng, C.Y., 1963. The San-i Overthrust. Petroleum Geol. Taiwan 2, 1–20.

Niwa, M., Shimada, K., Aoki, K., Ishimaru, T., 2016. Microscopic features of quartz and clay particles from fault gouges and infilled fractures in granite: discriminating between active and inactive faulting. Eng. Geol. 210, 180–196.

Niwa, M., Shimada, K., Ishimaru, T., Tanaka, Y., 2019. Identification of capable faults using fault rock geochemical signatures: a case study from offset granitic bedrock on the Tsuruga Peninsula, Central Japan. Eng. Geol. 260, 105235. https://doi.org/10.1016/j.enggeo.2019.105235.

Otuka, Y., 1936. The earthquake of Central Taiwan (Formosa), April 21, 1935 and earthquake faults. Bulletin of the Earthquake Research Institute, Tokyo Imperial University 3, 22–74.

Sinotech, 2017. National Highway No. 4 project investigation documentary and evaluation report (in Chinese). Taiwan Area National Expressway Engineering Bureau 267pp.

Suppe, J., 1981. Mechanics of mountain-building and metamorphism in Taiwan. Mem. Geol. Soc. China 4, 67–89.

Suppe, J., 1984. Kinematics of arc-continent collision, flipping of subduction, and back-arc spreading near Taiwan. Memoir of the Geol. Soc. China 6, 21–33.

Suppe, J., Namson, J., 1979. Fault-Bend Origin of Frontal Folds of the Western Taiwan Fold-and-Thrust Belt. Petroleum Geol. Taiwan 16, 1–18.

Tan, K., 1936. The Sansa overthrust, and the geological structure of the neighboring areas. Taiwan Tigaku Kizi 7 (1–3), 5–14.

Tang, C.H., 1969. Photogeologic interpretation of the Miaoli area, Taiwan, with special reference to its geologic structures. Proceedings of the Geological Society of China 12, 11–19.

Wang, C.Y., Chang, C.H., Yen, H.Y., 2000. An interpretation of the 1999 Chi-Chi earthquake in Taiwan based on the thin-skinned thrust model. Terr. Atmos. Ocean. Sci. 11 (3), 609–630. https://doi.org/10.3319/TAO.2000.11.3.609(CCE).

Wang, C.Y., Tanaka, H., Chow, J., Chen, C.C., Hong, J.H., 2002. Shallow reflection seismics aiding geological drilling into the Chelungpu fault after the 1999 Chi-Chi earthquake, Taiwan. Terr. Atmos. Ocean. Sci. 13 (2), 153–170. https://doi.org/10.3319/TAO.2002.13.2.153(T).

Wang, J.H., 2005. Earthquakes rupturing the Chelungpu fault in Taiwan are time predictable. Geophys. Res. Lett. 32, L06316. https://doi.org/10.1029/2004GL021884.

Yang, K.M., Huang, S.T., Wu, J.C., Ting, H.H., Mei, W.W., Lee, M., Hsu, H.H., Lee, C.J., 2007. 3D geometry of the Chelungpu thrust system in Central Taiwan: its implications for active tectonics. Terr. Atmos. Ocean. Sci. 18 (2), 143–181.

Yen, Y.C., 2014. Active fault supplementary geological investigation project report (in Chinese). Central Geological Survey 92 pp.

Yue, L.F., Suppe, J., Hung, J.H., 2005. Structural geology of a classic thrust belt earthquake: the 1999 Chi-Chi earthquake Taiwan (Mw = 7.6). J. Struct. Geol. 27 (11), 2058–2083. https://doi.org/10.1016/j.jsg.2005.05.020.